Continuous seasonal river ebullition measurements linked to sediment methane formation.

Richard Jeremy Wilkinson, Andreas Maeck[2], Zeyad Alshboul, Andreas Lorke*

University of Koblenz-Landau, Institute for Environmental Sciences, Fortstr. 7, 76829 Landau, Germany. Tel: +49 (6341) 280-31825. Fax: +49 (6341) 280-31-577. Email: wilkinson@uni-landau.de

[2] Senect – Geißler & Mäck GbR, Westring 21, Landau, Germany

Number of pages: 15 (including cover sheet)

Number of figures: 9

Number of tables: 3

Continuous seasonal river ebullition measurements linked to sediment methane formation.

Jeremy Wilkinson, Andreas Maeck[2], Zeyad Alshboul, Andreas Lorke*

Supporting information.

Background material

ME results from the dissolution of CH_4 produced in anoxic sediments into the surrounding porewater[1]. As this process continues, and due to low efflux rates, the porewater CH_4 concentration increases to the point at which the partial pressure of all dissolved gases exceeds the ambient pressure and surface tension of the water, and free gas is formed. With ongoing CH_4 formation, the bubbles grow and form fractures or disc-shaped cavities[2-3]. The gas produced leaves the sediment via diffusion and ebullition. Diffusion of dissolved CH_4 takes place at a relatively slow rate, which is further diminished by oxidization in the upper sediment layers[4]. ME is, in contrast, a relatively rapid process, rising bubbles bypass the upper sediment layers and generally avoid microbial oxidation, and hence a larger fraction of the initial CH_4 produced reaches the atmosphere[5]. In situations in which bubbles migrate slowly upward, other electron acceptors like O_2, NO_3, or SO_4 in the upper layers can cause re-dissolution and oxidization of CH_4, reducing the quantity passing into the water column[6]. The composition of gas bubbles released from anoxic freshwater sediments is dominated by CH_4[7], but the rising bubbles undergo a degree of loss by dissolution (gas exchange) into the water column. This is determined by the travel distance (water depth), bubble size, and concentration gradient (dissolved CH_4 concentration)[8-9].

Automated Bubble Traps (ABTs)

The ABTs required minimal maintenance and could be deployed over extended periods. They consist of an inverted polypropylene funnel with a diameter of 1 m, a gas holding cylinder, a differential pressure sensor (PD-9/0,1 bar FS, Keller AG), and a custom-made electronic unit (data logger and regulation device for venting the gas capture container). The submerged ABTs were suspended 0.5 m below a buoy, and held in a fixed location by two 9 m ropes with anchor weights deployed upstream and downstream, away from the measurement site (to minimize sediment disturbance below the collector funnel). The pressure transducer monitors the water level in the collection cylinder, based on the differential pressure between the inside and outside of the container as described by [10]. When full, a solenoid mechanism vents the cylinder automatically.

Model adjustment

The model was adjusted manually in sequence, firstly with $a_3 = 0$ (i.e., no oxygen offset), such that the exponential decay curves approximately fit the incubation decline data and the mean annual flux was greater than the mean annual ME. Oxygen offset was then adjusted to give a plausible depth profile, in terms of the depth and extent of oxygen effects. Further adjustments were made to the slope and magnitude of the exponential decline curves (again with $a_3 = 0$) to give MF = 0 at z = 0 (i.e., at the SWI). The area under the MF curve at 25 °C for each ABT was set to be proportional to 4 z_2 (i.e., the sediment depth, Table 2).

Table S1. Summary statistics for hourly mean ME data for sites in the Saar River (units - g CH_4 m^{-2} d^{-1}).

Site (river km)	ABT 1 (20 km)	ABT 2 (19.8 km)	ABT 3 (19.55 km)	ABT 4 Mettlach
N	6805	6601	5960	5080
Median	1.065	0.267	0.529	0.352
5th percentile	0.091	0.000	0.069	0.000
Mean	1.900	0.754	1.084	0.749
99th percentile	12.87	6.283	6.962	5.273
Maximum	57.58	33.07	15.60	9.614
St.Dev	2.773	1.606	1.444	1.072
CoV[a] (raw) %	146.0	213.1	133.2	143.2
CoV (smoothed) %	57.0	87.1	59.7	64.2
Winter - Oct to end March	1.08	0.28	0.43	0.27
Summer - April to end data	2.94	1.16	1.20	1.26
ratio (summer: winter)	2.75	4.51	2.73	3.69
Annual ME (g m^{-2} y^{-1})	694.8	275.7	396.3	273.9

[a]CoV – coefficient of variation = standard deviation / mean

Table S2. Parameters used to match simulated to measured ME, and resulting metrics related to the fit.

Parameter or metric	ABT 1	ABT 2	ABT 3	ABT 4[a]
Sediment depth, z_{sed} (m) = 17 sedimentation rate	4.93	1.19	1.7	1.243
Depth of high rate exponential decline, z_u (m)	0.18	0.1	0.15	0.09
Depth of low rate exponential decline, z_2 (m) = z_{sed} / 4	1.23	0.3	0.425	0.311
Methane loss (sigmoid) slope, b_3	0.90	0.50	0.95	0.57
High rate exponential decline multiplier, a_1	1.5	1	1.25	1.53
Low rate exponential decline multiplier, a_2	0.4	0.7	0.44	0.58
Methane loss (sigmoid) multiplier, a_3	2	1.9	2	2.4
Methane loss (sigmoid) depth shift, c_1	2.7	2.1	1.2	2
Flux from depth profile area at 25°C (g CH_4 m^{-2} d^{-1})	7.00	2.19	3.41	2.24
Methane loss (g O_2 m^{-2} d^{-1})	0.576	0.741	0.321	0.806
Bubble rise methane dissolution adjustment (bubble size 3.2 mm)	0.79	0.96	0.887	0.936

[a]ME measured ABT4 was not consistent with the accumulated sediment depth (2.55 m) and could not be fit with the model without applying very high methane loss (1.74 g O_2 m^{-2} d^{-1}). This anomaly may be due to dredging at that site, consequently, we adjusted the sediment depth according to the correlation of ABT deployment depth and sediment depth at the other sites (the results presented are based on the adjusted sediment depth).

Carbon burial

Carbon burial rate was estimated by calculating the total annual carbon deposited by sedimentation minus the carbon returned to the atmosphere by ebullition. The carbon deposited was estimated from the carbon content of the sediment core samples quantified CHNS analysis[1]. The emitted carbon was estimated from ME plus oxygen offset, plus an additional 20% for diffusive

emissions[1]. For the comparison with sedimentation rate, log10 (sedimentation rate in mm y^{-1}) was used following the approach of Sobek, et al.[11].

Table S3. Carbon burial estimated from annual methane formation (MF) and carbon deposition.

	ABT 1	ABT 2	ABT 3	ABT 4[a]
ME (g CH_4 m^{-2} y^{-1})	694.0	275.4	395.9	273.6
Methane loss (as g CH_4 m^{-2} y^{-1})	105.1	135.3	58.7	147.2
Bubble rise loss	0.79	0.96	0.887	0.936
MF before methane loss and bubble rise (g CH_4 m^{-2} y^{-1})	983.6	422.2	505.0	439.5
Total ebullition without losses (as kg C m^{-2} y^{-1})	**0.300**	**0.317**	**0.149**	**0.354**
Carbon input from sedimentation				
Sedimentation (m y^{-1})	0.29	0.07	0.10	0.15
Sediment C content (kg C m^{-3})	80.02	88.10	73.93	80.68
Carbon deposition (kg C m^{-2} y^{-1})	**23.21**	**6.17**	**7.39**	**12.10**
***C burial rate* (% y^{-1})**	***99.7***	***94.9***	***98.0***	***97.1***

[a]Note: Sedimentation rate at ABT 4 estimated (see note Table 2).

Sediment Incubation for MF

Sediment core sub-samples extracted from sealed cores were pushed upwards and removal from the desired depth using a slicer. This material was homogenized and 3 ml put into pre-weighed 250 ml flasks using an open ended 10 ml syringe. These were then sparged with nitrogen, sealed, and pressurized to the equivalent *in-situ* depth of water and sediment. Duplicate sub-samples were incubated at 5 preset temperatures (4, 10, 15, 20, and 25 °C, respectively); a total of 10 flasks per depth location. Figure S1 presents the incubation results.

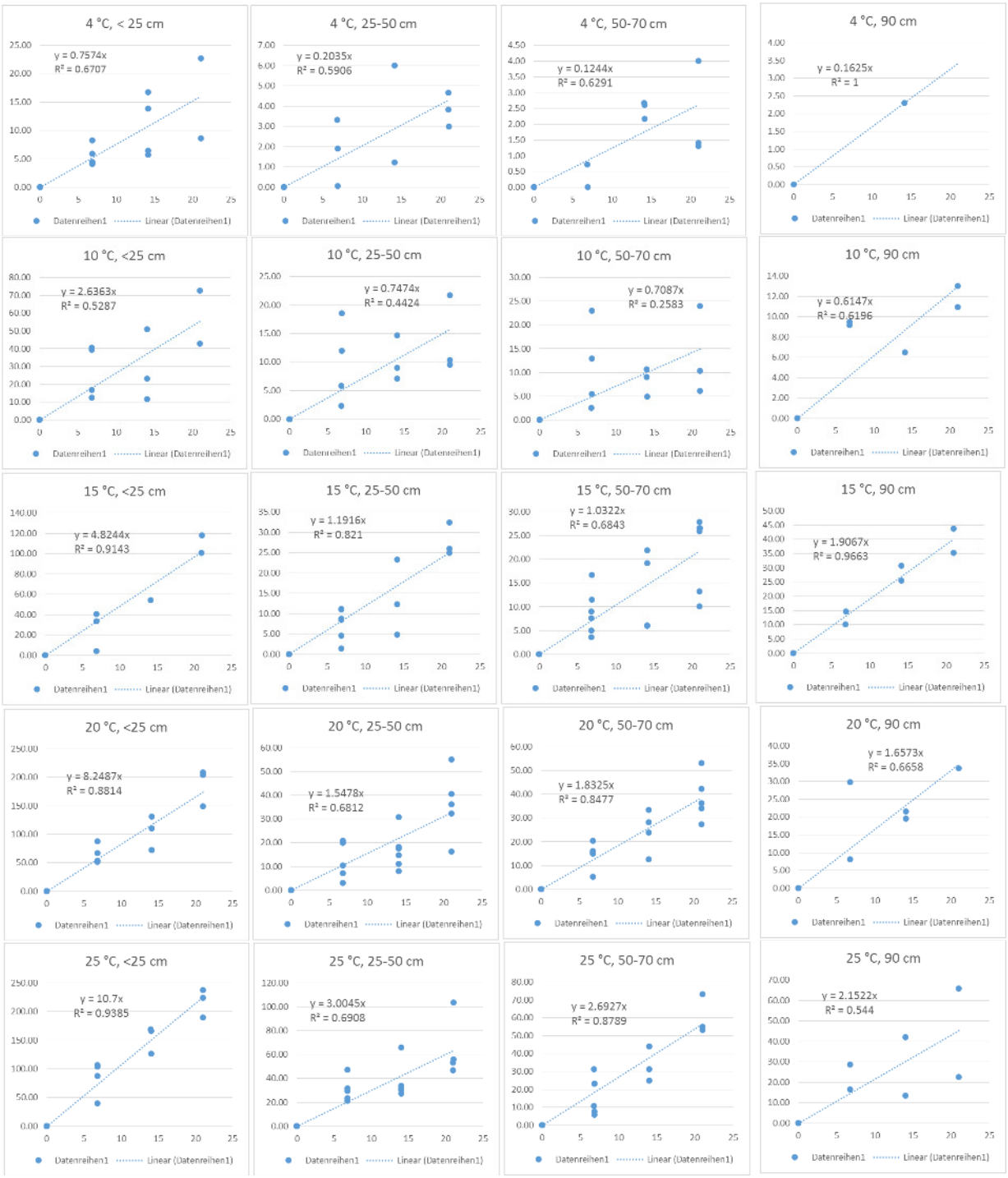

Figure S1. Results of the incubation experiments for MF grouped by treatment temperature and subsample depth, showing the increase in methane concentration over time from the beginning of the experiments.

We investigated several ways of analyzing and summarizing the results. The method presented was the most satisfactory approach and gives consistent results. The methane concentration at t = 0 was subtracted from all subsequent values and hence the increase in CH_4 with time could be plotted and linear regression curves fitted, the slopes of the curves were compared with the treatment temperature and sub-sample depth to give MF – depth and temperature relationships.

Periods of Zero ME in winter

We investigated the occurrence of periods without ebullition by summing the hours in each month and by site when no bubbles were collected, the results are presented in Figure S2, showing that the shallow water site ABT2 (2 m) exhibited the greatest total time without ebullition. The data for ABT4 was too patchy to analyse in this way. The occurrence of zero ebullition periods showed no strong pattern through the course of the day (Figure S3).

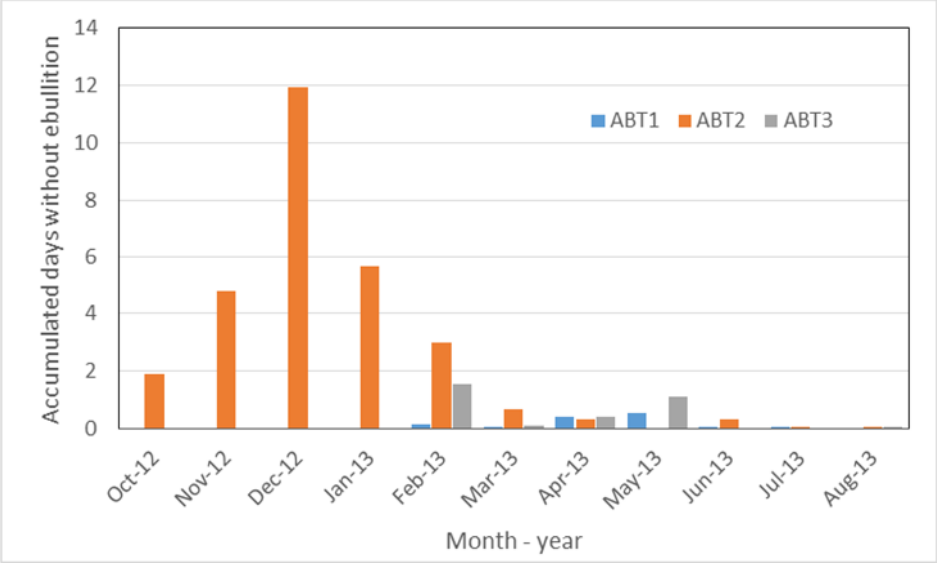

Figure S2. Summed hours with zero ebullition expressed as days by month.

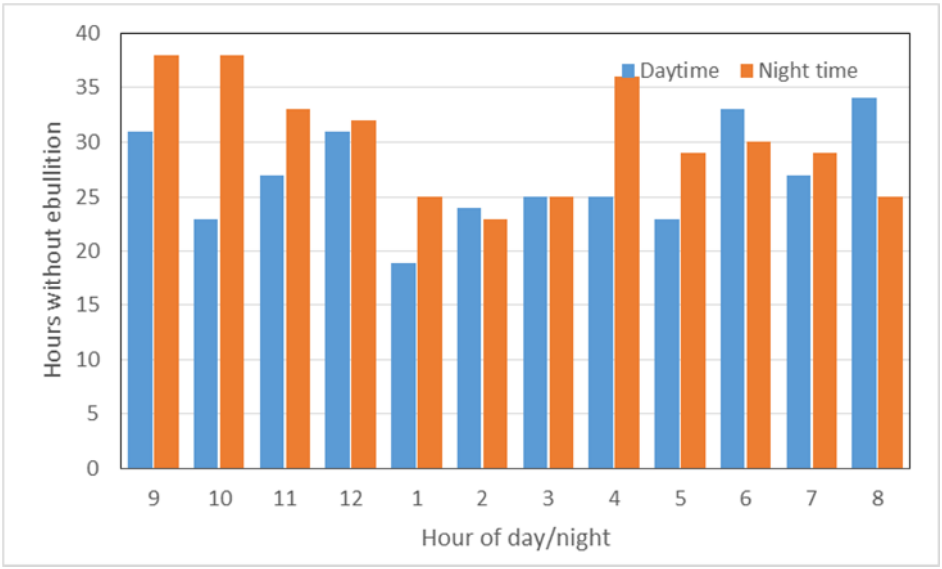

Figure S3. Occurrence of periods of zero-emission hours by hour of the day.

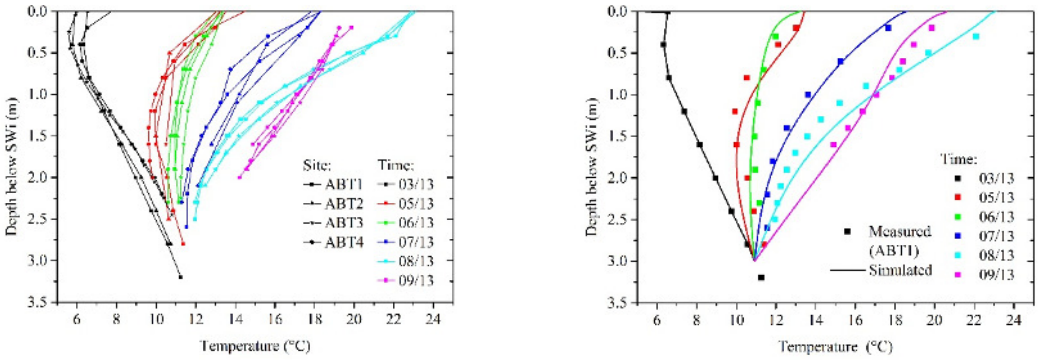

Figure S4. (A) Sediment temperature profiles measured from March to September 2013, and (B) measured vs. simulated sediment temperature.

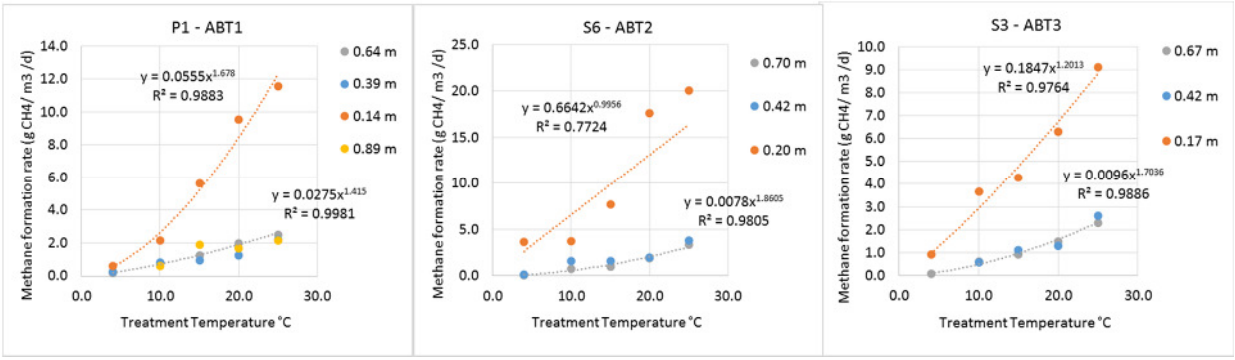

Figure S5. MF by temperature and depth for the individual cores (P1-ABT1, S3-ABT3, S6-ABT2).

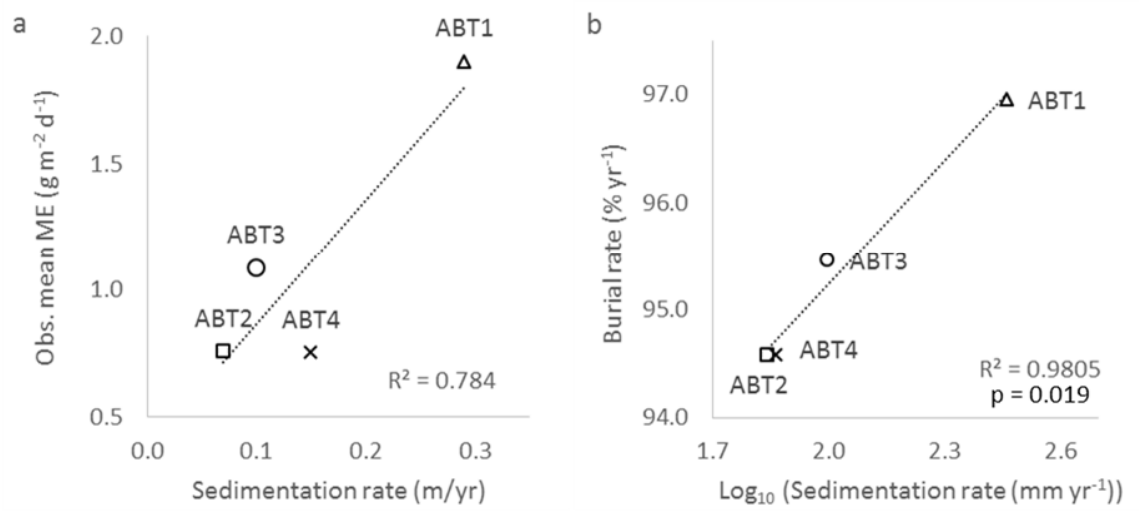

106

107 Figure S6. Relationships between (A) mean annual ME and sedimentation rate at each ABT site,

108 and (B) carbon burial rate and $\log_{10}$ sedimentation rate.

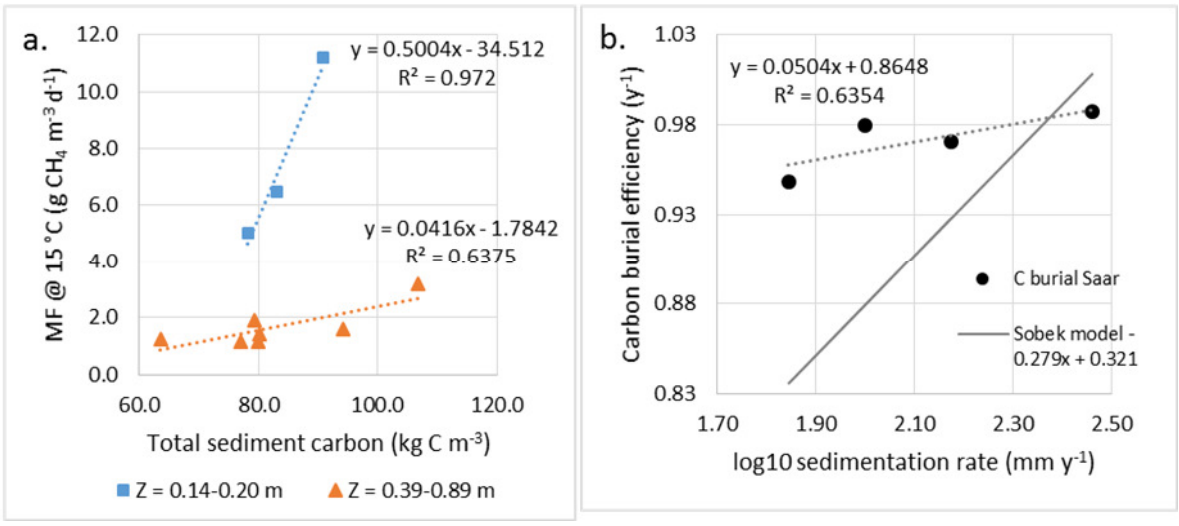

109

110 Figure S7. Incubation MF for three cores at 15 °C plotted by sub-sample depth (Z) versus sediment

111 C (kg C m^{-3}) (A). Note that the depth ranges represent the upper and lower bands from which

112 sediment cores were subsampled. (B) estimated carbon burial efficiency for the Saar ABT

113 ebullition monitoring sites versus $\log_{10}$ sedimentation rate (mm y^{-1}), plotted relative to the

114 relationship presented by Sobek et al.[11].

115

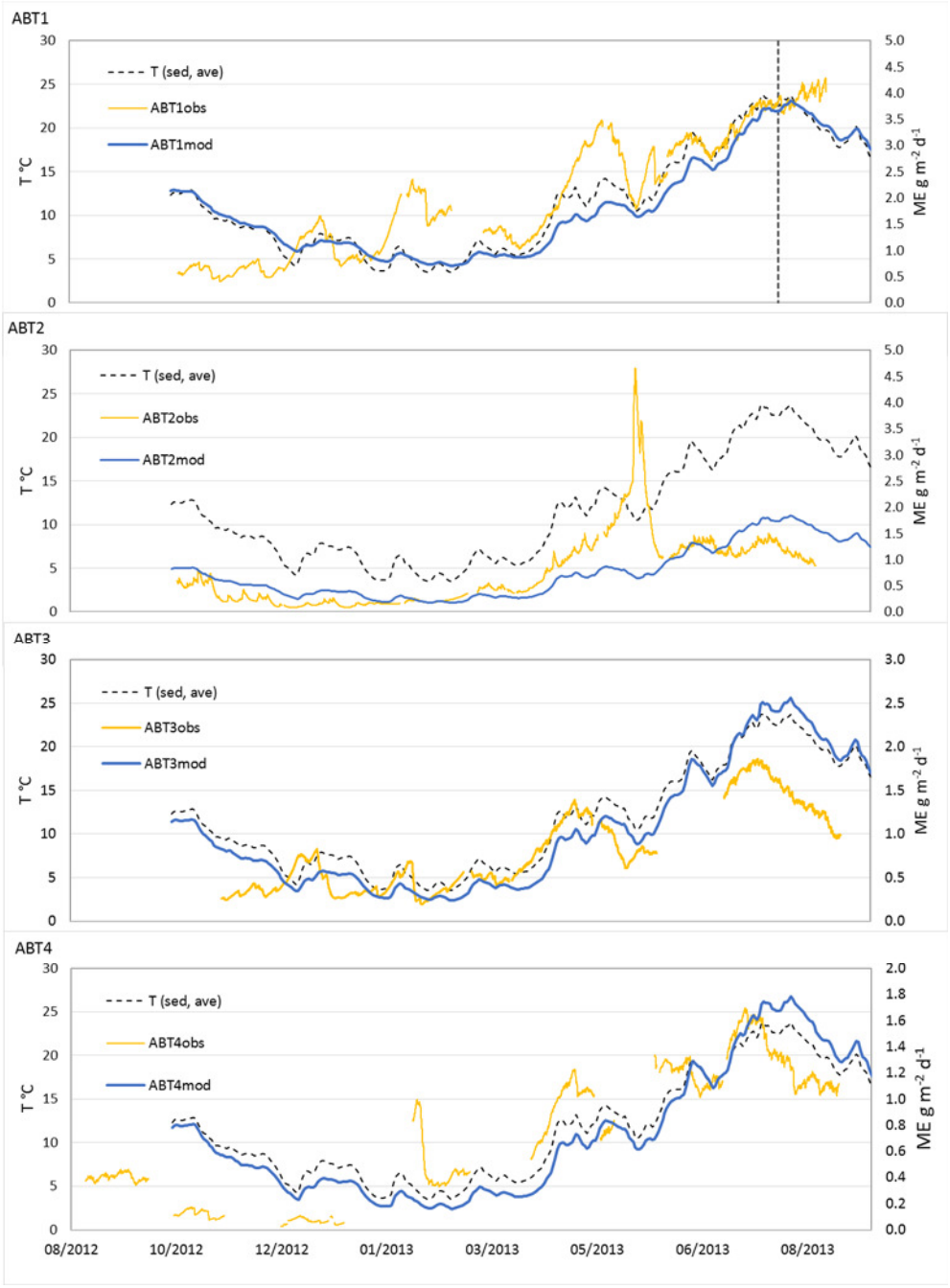

Figure S8. Simulated ME for each ABT location.

Figure S8 shows ME simulated from sediment temperature and settlement rate. Temperature alone determines the temporal variation of the curves. These are initial but satisfactory results, refinements to the model to incorporate other driving variables should improve the model fit.

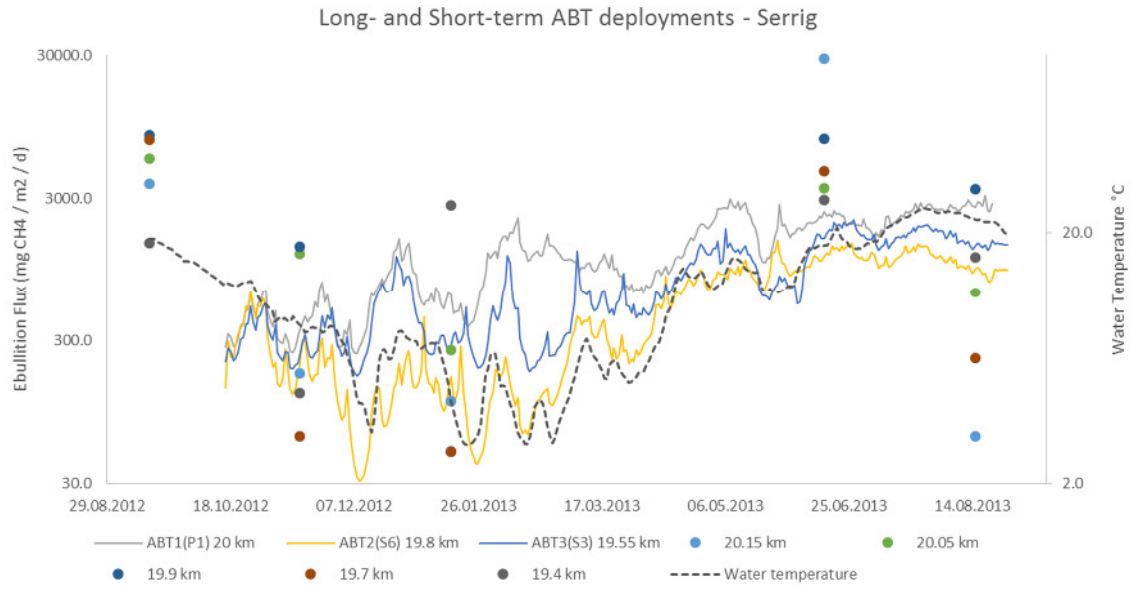

Figure S9. ABT flux records with previous short-term ME survey data showing elevated fluxes in late summer. This plot demonstrates the variability of short-term ME monitoring compared to continuous measurements.

Examining the divergence of our 2012-13 ABT data from simple temperature divergence we plotted short-term data from previous years with the new continuous data to see if low ebullition in September and October is a consistent pattern. Due to the temporal variability of ebullition, the short-term data do not offer an adequate comparison (Figure S9).

Ebullitive contribution to overall emissions

Maeck, et al.[1] estimated that ME across the air water interface accounted for about 40% of emissions, a further 40% was degassed after dams, and the remainder was released by water surface diffusion. ME was, however, proposed as the main pathway of release from the source sediments. If diffusion from the sediment is minor compared to ME, but degassing after dams is significant, the rise of bubbles must contribute to the dissolved methane concentration in the water

column. [1] demonstrated high water column dissolved CH_4 concentrations, and estimated loss from bubbles dissolution is up to 21% for the deeper ABT1 site[9]. Either bubble dissolution, enhanced diffusion, or enhanced advective pore water release, or all mechanisms together probably contribute to the elevated dissolved methane in the Serrig impoundment.

Seasonal gaseous expansion

Since the river sediment in the Saar experiences a seasonal temperature variation of about 10 °C averaged over 2 m of depth, the gas stored within the sediment would expand during spring and into summer, and contract from late summer into autumn and winter. With the declining temperature and possible carbon supply limitation, the gas production might be expected to drop off, and hence also the observed flux to the water column and subsequently the flux to the atmosphere. A change in temperature from 7 to 17 °C, however, would only increase the volume of a fixed mass of gas by approximately 3.5%.

Microbial controls on MF

The mechanisms and processes controlling MF may give insights into temporal variations in ME. MF is driven by a complex series of interactions in the sediment of which methanogenesis is the terminal step[12]. Methanogens require other anaerobes to break down complex organic compounds into fatty acids and simple sugars, which in-turn must be degraded by syntrophs, fermenters, and acetogens into hydrogen, carbon dioxide, formate, acetate, and methyl group compounds which are substrates usable by methanogens[13]. Subsequent to MF processes in the upper sediment consume CH_4, including methanotrophy (anaerobic methane oxidation - AMO)[13], nitrate/nitrite dependent AMO (found in deep water sediments)[14], and direct oxidation in the oxic zone.

Acetate substrate dominance

In some systems hydrogenotrophic methanogens will dominate methanogenesis, and in others acetogenotrophic types[12]. In temperate freshwater lakes acetate is the dominant (80-95%) MF substrate[15-17]. I the absence of acetate, Nozhevnikova, et al.[17], found that H_2/CO_2 was converted to acetate prior to methanogenesis. With temperatures increasing towards 30 °C, H_2 dependent methanogenesis can increase, as the relative activity of the contributing groups of microbes changes[16].

References:

(1) Maeck, A.; DelSontro, T.; McGinnis, D. F.; Fischer, H.; Flury, S.; Schmidt, M.; Fietzek, P.; Lorke, A., Sediment Trapping by Dams Creates Methane Emission Hot Spots. *Environmental Science & Technology* **2013,** *47* (15), 8130-8137.
(2) Boudreau, B. P.; Algar, C.; Johnson, B. D.; Croudace, I.; Reed, A.; Furukawa, Y.; Dorgan, K. M.; Jumars, P. A.; Grader, A. S.; Gardiner, B. S., Bubble growth and rise in soft sediments. *Geology* **2005,** *33* (6), 517-520.
(3) Johnson, B. D.; Boudreau, B. P.; Gardiner, B. S.; Maass, R., Mechanical response of sediments to bubble growth. *Marine Geology* **2002,** *187* (3), 347-363.
(4) Segers, R., Methane production and methane consumption: a review of processes underlying wetland methane fluxes. *Biogeochemistry* **1998,** *41* (1), 23-51.
(5) Kiene, R. P., Production and consumption of methane in aquatic systems. *Microbial production and consumption of greenhouse gases: Methane, nitrogen oxides and halomethanes. American Society for Microbiology* **1991**, 111-146.
(6) Venkiteswaran, J. J.; Schiff, S. L.; St Louis, V. L.; Matthews, C. J.; Boudreau, N. M.; Joyce, E. M.; Beaty, K. G.; Bodaly, R. A., Processes affecting greenhouse gas production in experimental boreal reservoirs. *Global Biogeochemical Cycles* **2013**.
(7) Baulch, H. M.; Dillon, P. J.; Maranger, R.; Schiff, S. L., Diffusive and ebullitive transport of methane and nitrous oxide from streams: Are bubble-mediated fluxes important? *Journal of Geophysical Research: Biogeosciences (2005–2012)* **2011,** *116* (G4).
(8) Leifer, I.; Patro, R. K., The bubble mechanism for methane transport from the shallow sea bed to the surface: A review and sensitivity study. *Continental Shelf Research* **2002,** *22* (16), 2409-2428.
(9) McGinnis, D.; Greinert, J.; Artemov, Y.; Beaubien, S.; Wüest, A., Fate of rising methane bubbles in stratified waters: How much methane reaches the atmosphere? *Journal of Geophysical Research: Oceans (1978–2012)* **2006,** *111* (C9).
(10) Varadharajan, C.; Hermosillo, R.; Hemond, H. F., A low-cost automated trap to measure bubbling gas fluxes. *Limnol. Oceanogr. Methods* **2010,** *8*, 363-375.

(11) Sobek, S.; Durisch-Kaiser, E.; Zurbrügg, R.; Wongfun, N.; Wessels, M.; Pasche, N.; Wehrli, B., Organic carbon burial efficiency in lake sediments controlled by oxygen exposure time and sediment source. *Limnology and Oceanography* **2009,** *54* (6), 2243-2254.
(12) Kallistova, A. Y.; Goel, G.; Nozhevnikova, A., Microbial diversity of methanogenic communities in the systems for anaerobic treatment of organic waste. *Microbiology* **2014,** *83* (5), 462-483.
(13) Nazaries, L.; Murrell, J. C.; Millard, P.; Baggs, L.; Singh, B. K., Methane, microbes and models: fundamental understanding of the soil methane cycle for future predictions. *Environmental microbiology* **2013,** *15* (9), 2395-2417.
(14) Deutzmann, J. S.; Stief, P.; Brandes, J.; Schink, B., Anaerobic methane oxidation coupled to denitrification is the dominant methane sink in a deep lake. *Proceedings of the National Academy of Sciences* **2014,** *111* (51), 18273-18278.
(15) Falz, K. Z.; Holliger, C.; Grosskopf, R.; Liesack, W.; Nozhevnikova, A.; Müller, B.; Wehrli, B.; Hahn, D., Vertical distribution of methanogens in the anoxic sediment of Rotsee (Switzerland). *Applied and Environmental Microbiology* **1999,** *65* (6), 2402-2408.
(16) Glissman, K.; Chin, K.-J.; Casper, P.; Conrad, R., Methanogenic pathway and archaeal community structure in the sediment of eutrophic Lake Dagow: effect of temperature. *Microbial Ecology* **2004,** *48* (3), 389-399.
(17) Nozhevnikova, A. N.; Nekrasova, V.; Ammann, A.; Zehnder, A. J.; Wehrli, B.; Holliger, C., Influence of temperature and high acetate concentrations on methanogenensis in lake sediment slurries. *FEMS microbiology ecology* **2007,** *62* (3), 336-344.